Revision 1.

Pressure-temperature stability studies of FeOOH using x-ray diffraction.

A. E. Gleason[1], R. Jeanloz[1], M. Kunz[2]

[1]Department of Earth and Planetary Science, University of California, Berkeley, McCone Hall # 4767, Berkeley, CA 94720

[2]Advanced Light Source, Lawrence Berkeley National Laboratory, 1 Cyclotron Road, Berkeley, CA 94720, USA.

ABSTRACT

The Mie-Grüneisen formalism is used to fit a Birch-Murnaghan equation of state to high-temperature (*T*), high-pressure (*P*) x-ray diffraction unit-cell volume (*V*) measurements on synthetic goethite (α-FeOOH) to combined conditions of T = 23-250^{o} C and P = 0-29.4 GPa. We find the zero-pressure thermal expansion coefficient of goethite to be α_0 = 2.3 (± 0.6) $\times 10^{-5} K^{-1}$ over this temperature range. Our data yield zero-pressure compressional parameters: V_0 = 138.75 (± 0.02) Å^3, bulk modulus K_0 = 140.3 (± 3.7) GPa, pressure derivative K_0' = 4.6 (± 0.4), Grüneisen parameter γ_0 = 0.91 (± 0.07), and Debye temperature Θ_0 = 740 (± 5) K. We identify decomposition conditions for 2α-FeOOH → α-Fe_2O_3 + H_2O at 1 – 8 GPa and 100 – 400^{o} C, and the polymorphic transition from α-FeOOH (*Pbnm*) to ε-FeOOH (*P2$_1$mn*). The non-quenchable, high-pressure ε-FeOOH phase *P*-*V* data are fitted to a second-order (Birch) equation of state yielding, K_0 = 158 (± 5) GPa and V_0 = 66.3 (± 0.5) Å^3.

Keywords: GOETHITE, XRD DATA, DIAMOND ANVIL CELL, COMPRESSIBILITY MEASURESMENTS

INTRODUCTION

Goethite, hematite (α-Fe_2O_3), maghemite (γ-Fe_2O_3), and lepidocrocrite (γ-FeOOH) represent the majority of crystalline ferric oxides and oxyhydroxides at Earth's surface. These minerals are abundant in soils, banded iron formations, iron ores and hydrothermal deposits. Understanding the stability and properties of simple hydroxides at high pressures and temperatures offers an important first step toward quantifying more complex hydrogen-bearing compounds relevant to the Earth's interior (e.g., Williams and Hemley 2001). We focus on iron-oxy-hydroxide because Fe is a major chemical component of the deep Earth, with valence (hence chemical-bonding properties) dependent on pressure. Also, goethite and hematite have been identified on the surface of Mars (Morris et al. 2004). The nature and properties of iron oxides and oxyhydroxides are therefore relevant to geochemistry, mineralogy and planetary science.

Thermodynamic properties and particle-size effects have been studied extensively for the goethite-hematite reaction (Langmuir 1971; Majzlan et al. 2003a; Majzlan et al. 2003b). Only recently was a detailed structural analysis of a natural crystal of goethite performed at ambient conditions, including anisotropic atomic-displacement parameters (Yang et al. 2006). Several investigations of the structural behavior of goethite at different conditions have been completed: Voigt and Will (1981) up to 10 GPa and 500^o C; Gualtieri and Venturelli (1999) to 800^o C at zero pressure; and Nagi et al. (2003) to 24.5 GPa at room temperature. Using routine high-pressure techniques, we present a pressure-temperature phase diagram and derive basic thermodynamic parameters for goethite.

EXPERIMENTAL PROCEDURE

A Bragg-(G) diamond cell (Diacell Products Ltd.), including diamonds with 200 µm culets and tungsten carbide backing plates, was resistively heated using a circular, internal heater with coils of Pt-30% Rh wire threaded in a pyrophyllite ring. A Chromel-Alumel thermocouple was in contact with the diamond to allow temperature measurements, while a West 6100 three-term controller was used to maintain the cell at constant temperature. The temperature was held constant to within one degree, but ambiguities in the placement of the thermocouple on the diamond facet, throughout repeated compression and decompression, resulted in an overall uncertainty of ± 10% in temperature as calculated from a two-thermocouple calibration (Ming et al. 1983). Our calibration consisted of two thermocouples, one between the diamond culets (TC1) and one where the distance of the thermocouple from the diamond facet varied (TC2). A calibration curve was established between TC1 and TC2, with the spread in TC2 values for a given temperature, due to position changes, providing an estimate of the uncertainty. During the actual experiment, only TC2 is used at elevated pressures, but from the calibration curve we can relate this back to a temperature measured at the location of the sample between the diamonds. It should be noted that we tried to mitigate the movement of TC2 by adhering it to a diamond facet at the start of the experiment. However, over the course of increasing and decreasing pressure and simultaneous heating, the DAC components shift – and in many cases, when we completed the experiment and opened the DAC, TC2 was no longer in that same initial position. We consider this fact when reporting temperatures. Rhenium gaskets were pre-indented to a thickness of 50 µm, and a hole of 125 µm served as the pressure chamber. Angle-dispersive powder-diffraction measurements were made on beamlines 11.3.1 and 12.2.2 at the Advanced Light Source.

On beamline 11.3.1 we used 0.730 Å x-rays with a beam-spot size of 100 µm x 100 µm and a Bruker CCD detector. Data acquisition times of 10-30 minutes were found to be sufficient to give data having adequate counting statistics. On beamline 12.2.2 (Kunz et al. 2005), patterns were collected using 0.414 - 0.497 Å x-rays and a beam-spot size of 50 µm x 50 µm with a MAR345 Image Plate. Data acquisition times of 30 minutes were found to be adequate. We first collected a set of high-pressure data at ambient temperature on a sample of finely ground synthetic goethite (courtesy of R. Morris, NASA, Johnson Space Center) and gold mixed 7:1 by weight and using non-dried 4:1 methanol-ethanol as the pressure transmitting fluid, similar to Nagi et al. (2003). Methanol-ethanol was also used at high temperatures. Ruby (Mao et al. 1978), NaCl (Birch 1986) and gold (Shim et al. 2002) were used as internal pressure standards for ambient-temperature compression, and only gold for the high-temperature runs.

Data were collected up to 29.4 GPa at ambient temperature and up to 21 GPa at temperatures of 100-400^{o} C, on compression and decompression along isotherms in 50 ^{o}C increments. To remain mostly in the stability field of goethite, we followed the dehydration boundary presented in Majzlan et al. (2003b). Once a target pressure-temperature condition was achieved, the sample would stay at that condition for 30 minutes or less, depending on whether a CCD or image plate was used to record the pattern. Two-dimensional diffraction images were reduced to one-dimensional patterns using the FIT2D program (Hammersley et al. 1996). Goethite (α-FeOOH) (Fig. 1a), and the high-pressure ε-FeOOH phase (Fig. 1b) were modeled using orthorhombic space groups *Pbnm* and $P2_1mn$, respectively. The unit-cell parameters of each FeOOH phase and the pressure calibrant were determined using Rietveld whole-pattern refinement

(Rietveld 1969), within the program GSAS (Larson and Von Dreele 1994) using the EXPGUI interface (Toby, 2001): R-factors for the fits were of the order of 5%.

RESULTS

The high-pressure lattice parameters (Fig. 2) and volumes (Fig. 3a) of goethite at ambient temperature and high temperatures are contained in MSA Depository Table 1. We did perform separate peak fitting of the 200^{o} C isotherm data using the PeakFit Program (Jandel Scientific, San Rafael, CA), from which we calculated cell parameters. The results from PeakFit were the same as from GSAS, within mutual errors. In general, the lengths of the crystallographic axes decrease with increasing pressure. The *a*-axis length decreases smoothly up to roughly 9 GPa, beyond which it diverges from Nagai et al.'s (2003) trend and follows a slope of -0.009 Å GPa^{-1}; the compression and decompression trends are similar. The *b*-axis length decreases smoothly with pressure up to 9 GPa, followed by a 0.02 Å discontinuity over a pressure range of 5 GPa and then returns to match Nagai et al.'s (2003) trend. The *c*-axis length decreases smoothly with pressure to 9 GPa, followed by increased scatter, up to ± 0.01 Å. Decompression data demonstrate hysteretic effects for the *b*- and *c*- axes.

The volume compression at room temperature shows a smooth decrease up to 9 GPa, followed by a discontinuity and then returns to a smooth trend up to 24.6 GPa. The higher-temperature isotherms maintain a smooth decrease in volume through the room-temperature 9 GPa discontinuity. We attribute this 9 GPa kink in room-temperature volumes and lattice parameters to the solidification of the 4:1 methanol:ethanol pressure medium introducing non-hydrostaticity. The temperature dependence of the glass-transition pressure in methanol:ethanol (Grocholski and Jeanloz 2005) explains the lack

of the discontinuity in the high-temperature data. The lattice parameters and volumes (Fig. 3b) for ε-FeOOH phase are listed in MSA Depository Table 2. The decrease in volume for any isotherm does not follow a single smooth trend, with scatter up to ± 0.3 $Å^3$ over the entire pressure range.

DISCUSSION

The thermal equation of state for goethite is generated by combined use of the Mie-Grüneisen and Eulerian finite-strain (Birch-Murnaghan) (Birch 1978) equation of state

$$P(V,T) = 3K_0 f[(1+2f)^{5/2}(1-2\left[\frac{3}{4}(K_0'-4)\right]f + \frac{\gamma}{V}\left[E(T,\Theta)-E(300,\Theta)\right] \qquad (1)$$

relating pressure, *P*, volume, *V*, bulk modulus, *K*, and its pressure derivative, *K'*, using volumetric finite strain, $f = 1/2[(V_0/V)^{2/3}-1]$, the Gruneisen parameter $\gamma = -(\partial \ln\Theta/\partial \ln V)_T$, internal energy *E* at temperature *T*, the Debye temperature Θ, and subscript *0* to indicate ambient pressure. The parameter values are given in Table 1. We include all *P-V-T* data in determining K_0 = 140.3 (± 3.7) GPa and K_0'= 4.6 (± 0.4), as the accuracy of high-temperature data at pressure prevented resolving volumetric expansion as temperature was increased up to 250 ^oC. Nagai et al. (2003) report a bulk modulus of 111(2) GPa, but this difference is likely due to variable degrees of non-hydrostaticity. A compression study with a pressure-transmitting medium other than methanol:ethanol, or high temperatures (as in the present study), may be required to mitigate non-hydrostatic effects. We find that goethite has a slightly larger bulk modulus than the iso-structural main-element analogue, diaspore, α-AlOOH (K_0 = 134.4 ±1.4 GPa, assuming K_0' = 4: Grevel et al. (2000)). At *P* = 0 GPa, we find the zero-pressure thermal expansion coefficient of goethite to be comparable to that of diaspore ($\alpha = 2.9(2)\cdot10^{-5}K^{-1}$ Grevel et

al. 2000). Assuming $d\ln\gamma/d\ln V = 1.0$, using the thermodynamic relationship $\gamma_0 = \alpha_0 K_0 V C_V^{-1}$ (Jeanloz 1985), where C_V is the isochoric heat capacity, and following from a Debye specific heat function table (Pitzer 1995), we find $\Theta_0 = 740$ (± 5) K for goethite.

It should be noted that a secondary data analysis for each phase was performed, wherein high-temperature data were separated in two distinct ways: 1) all high-temperature data grouped together, separate from room-temperature measurements; and 2) each isotherm assessed individually. The expected trend of 'softening' or decrease of bulk modulus with increasing temperature was not found, and scatter in the finite-strain data made it inappropriate to judge trends in isothermal bulk modulus at high temperature. This is especially true for the ε-FeOOH phase and, as a first order investigation of this phase, we chose to report the results for the simplest analysis.

For the high-pressure ε-FeOOH phase, the Birch equation of state was used to determine the bulk modulus, K_0 =158 ±5 GPa with K_0' assumed to be 4. Scatter in the high-temperature data and lack of any apparent trend in volumetric thermal expansion from one isotherm to another warranted including all data in the determination of the bulk modulus. Ambient-pressure, room-temperature volume for this non-quenchable high pressure ε-FeOOH phase is determined using the *G* vs. *g* method (Jeanloz 1981). The calculated zero-pressure volume is $V_{\varepsilon 0} = 66.3$ (± 0.5) Å^3. The iso-structural high-pressure AlOOH phase with space group $P2_1nm$ is δ-AlOOH (Suzuki et al. 2000), with an isothermal zero-pressure bulk modulus of 252(3) GPa (Vanpeteghem et al. 2002). We note that the Al-bearing phase is roughly 2/3 less compressible than the ε-FeOOH high-pressure phase.

A summary of experimental data from the present study and Voigt and Will's (1981) work (Fig. 4) includes an expanded pressure-temperature stability range for the high-pressure ε-FeOOH phase, and validation of the reaction boundary between goethite and hematite + water. The phase boundary between α-FeOOH and ε-FeOOH has been further constrained by the data presented here, and α-FeOOH is only metastable at low temperatures. A phase boundary nearly independent of temperature (200-250 ^{o}C between 6-20 GPa) is thermodynamically unreasonable, given the fact that our data also reinforce the temperature-dependent α- to ε-FeOOH boundary proposed by Voigt and Will (1981) (dashed black line in Figure 4). We believe the temperature independent discontinuity is a kinetic artifact related to the polymorphic conversion from space group *Pbnm* to $P2_1mn$. We note the appearance of lepidocrocite (γ-FeOOH) diffraction peaks between 200-250 ^{o}C at 2-9 GPa, which may also act to stabilize goethite to higher pressures and temperatures. At conditions below 200 ^{o}C and above 5 GPa, α-FeOOH may only be metastable and convert, with longer reaction times, to ε-FeOOH. The similarity of the thermoelastic properties of α-AlOOH (Grevel et al. 2000) and α-FeOOH (this study) suggests that at lower pressures (~5 GPa, corresponding approximately to the base of the lithosphere), at least for this structure type, the thermoelastic properties are dominated by the common structure type rather than the chemical difference between Al and Fe (e.g. transition metal vs. main-group element). However, at pressure up to 10-25 GPa (corresponding to the upper mantle and transition zone), differences in the elastic properties of iso-structural ε-FeOOH and δ-AlOOH phases could be dominated by chemical differences between Al and Fe.

ACKNOWLEDGEMENTS

Financial support for this study was provided by the National Science Foundation Graduate Research Fellowship 2004016305 to A.E. Gleason; The Advanced Light Source is supported by the Director, Office of Science, Office of Basic Energy Sciences, of the U.S. Department of Energy under Contract No. DE-AC02-05CH11231. We are grateful for the help and assistance of W. Caldwell and S. Fakra. And we thank the anonymous reviewers and Associate Editor George Morgan for their constructive comments to improve the manuscript.

REFERENCES

Birch, F. (1978) Finite strain isotherm and velocities for single crystal and polycrystalline NaCl at high pressures and 300^{o}K. Journal of Geophysical Research, 83, 1257-1268.

Birch, F. (1986) Equation of state and thermodynamic parameters of NaCl to 300 Kbar in the high-temperature domain. Journal of Geophysical Research, 91B, 4949-4954.

Dyuzheva, T.I., Lityagina L.M., Nikolaev, N.A., Martynov, B.N., and Bendeliani, N.A. (2006) Growth of Single Crystals of High-Pressure epsilon-FeOOH Phase. Crystallographic Reports, 51, 342–343.

Grevel, K.D., Burchard, M., and Faβhauer, D.W. (2000) Pressure-volume-temperature behavior of diaspore and corundum: An in situ X-ray diffraction study comparing different pressure media. Journal of Geophysical Research, 105, 27877-27887.

Grocholski, B. and Jeanloz, R. (2005) High-pressure and –temperature viscosity measurements of methanol and 4:1 methanol:ethanol solution. Journal of Chemical Physics, 123, 204503.

Gualtieri, A.F. and Venturelli P. (1999) In situ study of goethite-hematite phase transition by real time synchrotron powder diffraction. American Mineralogist, 84, 895–904.

Hammersley, A.P., Svensson, S.O., Hanfland, M., Fitch, A.N., and Häusermann, D. (1996) Two-Dimensional Detector Software: From Real Detector to Idealized Image or Two-Theta Scan. High Pressure Research, 14, 235-248.

Jeanloz, R. (1981) Finite-strain equation of state for high-pressure phases. Geophysical

Research Letters, 8, 1219-1222.

Jeanloz, R. (1985) Thermodynamics of Phase Transitions. In S.W. Kieffer and A. Navrotsky, Eds., Atomic Environments to Mineral Thermodynamics, 389 p. Reviews in Mineralogy, Mineralogical Society of America, Washington, D. C.

Kunz, M., MacDowell, A.A., Caldwell, W.A., Cambie, D., Celestre, R.S., Domning, E.E., Duarte, R.M., Gleason, A.E., Glossinger, J.M., Kelez, N., Plate, D.W., Yu, T., Zaug, J.M., Padmore, H.A., Jeanloz, R., Alivisatos, A.P., and Clark, S.M. (2005) A beamline for high-pressure studies at the Advanced Light Source with a superconducting bending magnet as the source. Journal of Synchrotron Radiation, 12, 650-658.

Langmuir D. (1971) Particle size effect on the reaction: goethite = hematite + water. American Journal of Science, 271, 147–156.

Larson, A.C. and Von Dreele, R.B. (1994) GSAS, General Structure Analysis System, Los Alamos National Laboratory, LAUR, 86-748.

Majzlan J., Lang B., Stevens R., Navrotsky A., Woodfield B., and Boerio-Goates J. (2003a) Thermodynamics of Fe oxides: Part I. Entropy at standard temperature and pressure and heat capacity of goethite (alpha-FeOOH), lepidocrocite (gamma-FeOOH), and maghemite (gamma-Fe2O3). American Mineralogist, 88, 846–854.

Majzlan J., Grevel K., and Navrotsky A. (2003b) Thermodynamics of Fe oxides: Part II. Enthalpies of formation and relative stability of goethite (alpha-FeOOH), lepidocrocite (gamma-FeOOH), and maghemite (gamma-Fe2O3). American Mineralogist, 88, 855–859.

Mao, H.K., Bell, P.M., Shaner, J.W., and Steinberg, J. (1978) Specific volume

measurements of Cu, Mo, Pd, and Ag and calibration of the R1 fluorescence pressure gauge from 0.06 to 1 Mbar. Journal of Applied Physics, 49, 3276-3283.

Ming, L.C., Manghnani, M.H., Balogh, J., Qadri, S.B., Skelton, E.F., and Jamieson, J.C. (1983) Gold as a reliable internal pressure calibrant at high temperatures. Journal of Applied Physics, 54, 4390-4397.

Morris, R., Klingelhofer, G., Bernhardt B., Schroder, C., Rodionov, D., de Souza Jr., P., Yen, A., Gellert, R., Evlanov, E., Foh, J., Kankeleit, E., Gutlich, P., Ming, D., Renz, F., Wdowiak, T., Squyres, S., and Arvidson, R. (2004) Mineralogy at Gusev Crater from the Mossbauer Spectrometer on the Spirit Rover. Science, 305, 833–836.

Nagai, T., Kagi, H., and Yamanaka, T. (2003) Variation of hydrogen bonded O…O distances in goethite at high pressure. American Mineralogist, 88, 1423-1427.

Pitzer, K. (1995) Thermodynamics, 500 p. McGraw-Hill, New York, U.S.A.

Rietveld, H.M. (1969) A Profile Refinement Method for Nuclear and Magnetic Structures Journal of Applied Crystallography, 2, 65-71.

Shim, S., Duffy, T., and Kenichi, T. (2002) Equation of state of gold and its application to the phase boundaries near 660 km depth in Earth's mantle. Earth and Planetary Science Letters, 203, 729-739.

Suzuki, A., Ohtani, E., and Kamada, T. (2000) A new hydrous phase δ-AlOOH synthesized at 21 GPa and 1000 ^{o}C. Physics and Chemistry of Minerals, 27, 689-693.

Toby, B.H. (2001) EXPGUI, a graphical user interface for GSAS, Journal of Applied Crystallography, 34, 210–213.

Vanpeteghem, C.B., Ohtani, E., and Kondo, T. (2002) Equation of state of the hydrous phase δ-AlOOH at room temperature up to 22.5 GPa. Geophysical Research Letters, 29, 1119-1121.

Voigt, R. and Will, G. (1981) The system Fe_2O_3-H_2O under high pressures. Neues Jahrbuch für Mineralogie, 2, 89–96.

Williams, Q. and Hemley, R.J. (2001) Hydrogen in the Deep Earth. Annual Reviews of Earth and Planetary Sciences, 29, 365–418.

Yang, H., Lu, R., Downs, R.T., and Costin, G. (2006) Goethite, alpha-FeO(OH), from single-crystal data. Acta Crystallographica, inorganic papers, E62, i250-i252.

FIGURE CAPTIONS:

Figure 1. a) X-ray diffraction pattern of goethite and gold at ambient pressure and temperature; λ = 0.4133 Å. All Bragg peaks are indexed, although only a few are labeled here. b) X-ray diffraction pattern of high-pressure ε-FeOOH phase and gold at 17.2 GPa and 250 ^{o}C; λ = 0.4133 Å. The intensity in each pattern is in arbitrary units (a.u.). The black, dashed-grey and solid-grey curves are the experimental data, GSAS model fit and difference plot, respectively.

Figure 2. Refined orthorhombic unit cell parameters (*a, b, c*) for goethite at room temperature from this study (black circles) compared to the Nagai et al. 2003 dataset (grey circles). Solid circles represent compression, open circles are decompression. Error bars are 95% confidence limits for the unit-cell refinements.

Figure 3. a) Unit-cell volume of goethite as a function of pressure and temperature; solid symbols are for compression, open symbols for decompression. The curve is calculated from the third-order Birch-Murnaghan equation of state. Data resolution prohibited the determination of thermal expansivity at pressure. b) Unit-cell volume of ε-FeOOH phase as a function of pressure and temperature; solid symbols are for compression, open symbols for decompression. The curve is calculated from the second-order (Birch) equation of state (i.e., assuming $K_0' = 4$).

Figure 4. Pressure-temperature phase-stability diagram for FeOOH. Solid symbols are for compression, open symbols are for decompression. Black and grey symbols are the datasets from this study and Voigt and Will (1981), respectively. Solid and dashed lines at higher temperatures mark experimentally determined phase boundaries.

TABLES:

TABLE 1. Thermodynamic properties of goethite at zero pressure and 296 K.

V_0 [Å^3]	K_0 [GPa]	α_0 [$\times 10^{-5}$K^{-1}]	C_P[J/K·mol]	γ_0	Θ [K]
138.75 ±0.02	140.3 ±3.7	2.3 ±0.6	73.88*	0.91 ±0.07	740 ±5
*calculated from summed Debye and Einstein $C_P(T)$ functions (Majzlan et al. 2003a)					

FIGURES:

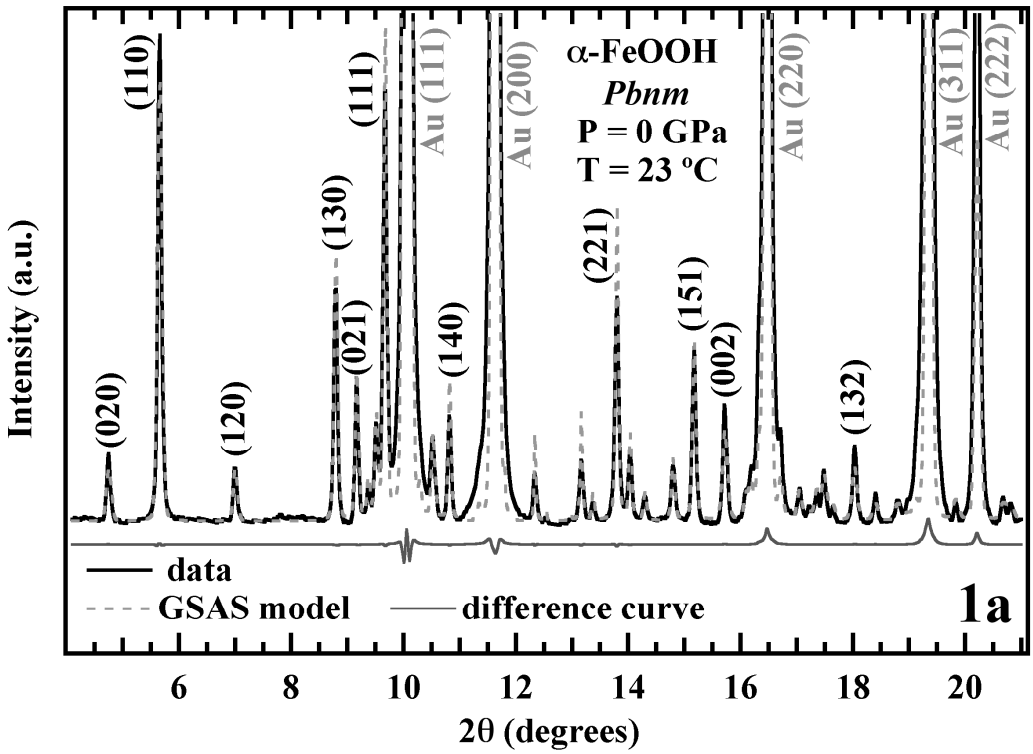

Figure 1a.

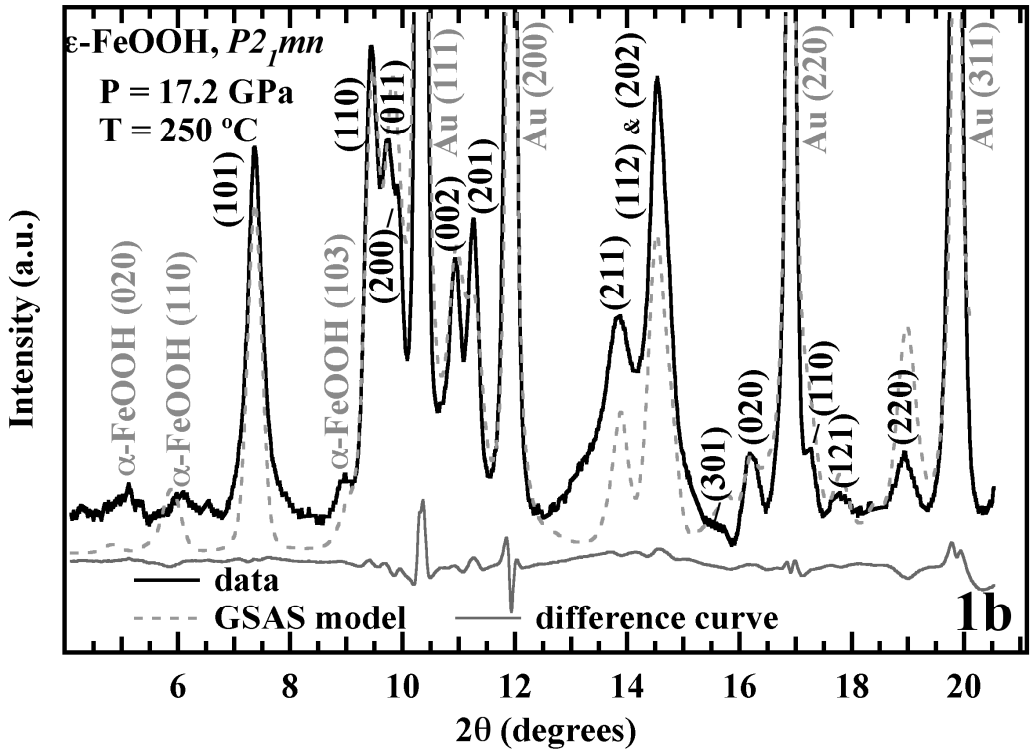
ε-FeOOH, P2₁mn
P = 17.2 GPa
T = 250 °C
Intensity (a.u.)
α-FeOOH (020)
α-FeOOH (110)
(101)
α-FeOOH (103)
(110)
(200)
(011)
Au (111)
(002)
(201)
Au (200)
(211)
(112) & (202)
(301)
(020)
Au (220)
(110)
(121)
(220)
Au (311)
data
GSAS model
difference curve
1b
6
8
10
12
14
16
18
20
2θ (degrees)

Figure 1b.

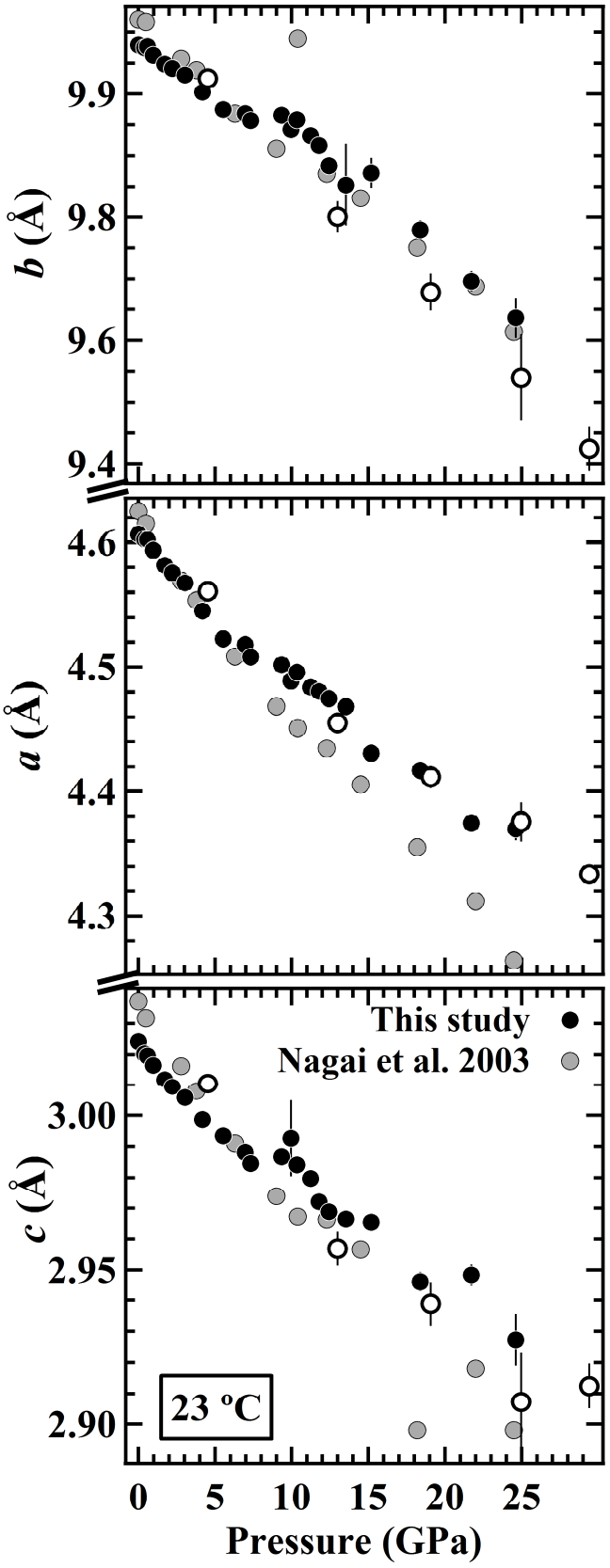
9.9
9.8
9.6
9.4
b (Å)
4.6
4.5
4.4
4.3
a (Å)
This study
Nagai et al. 2003
3.00
2.95
2.90
c (Å)
23 °C
0
5
10
15
20
25
Pressure (GPa)

Figure 2.

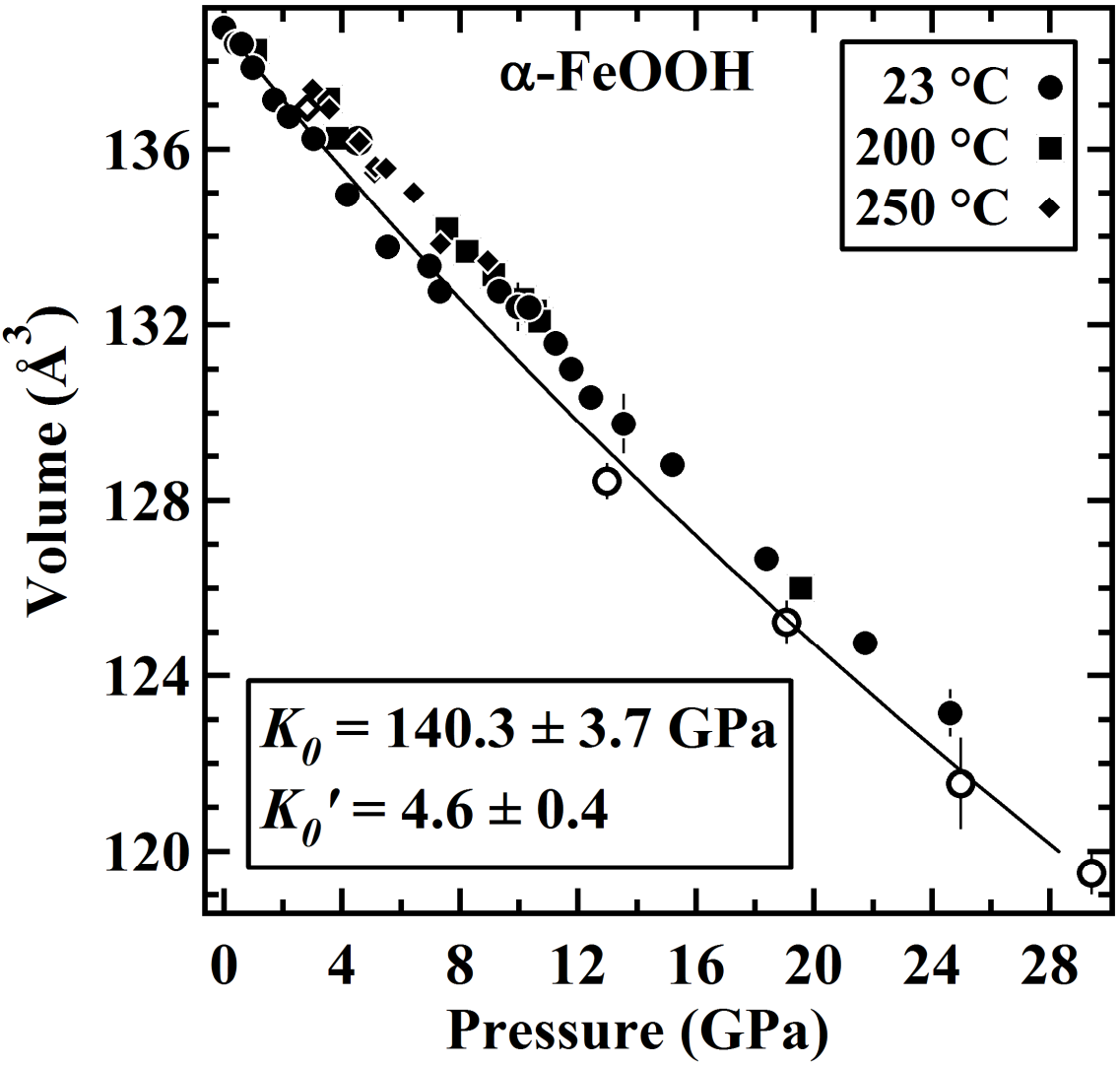
α-FeOOH
23 °C
200 °C
250 °C
K_0 = 140.3 ± 3.7 GPa
K_0' = 4.6 ± 0.4
Volume (Å^3)
136
132
128
124
120
0
4
8
12
16
20
24
28
Pressure (GPa)

Figure 3a.

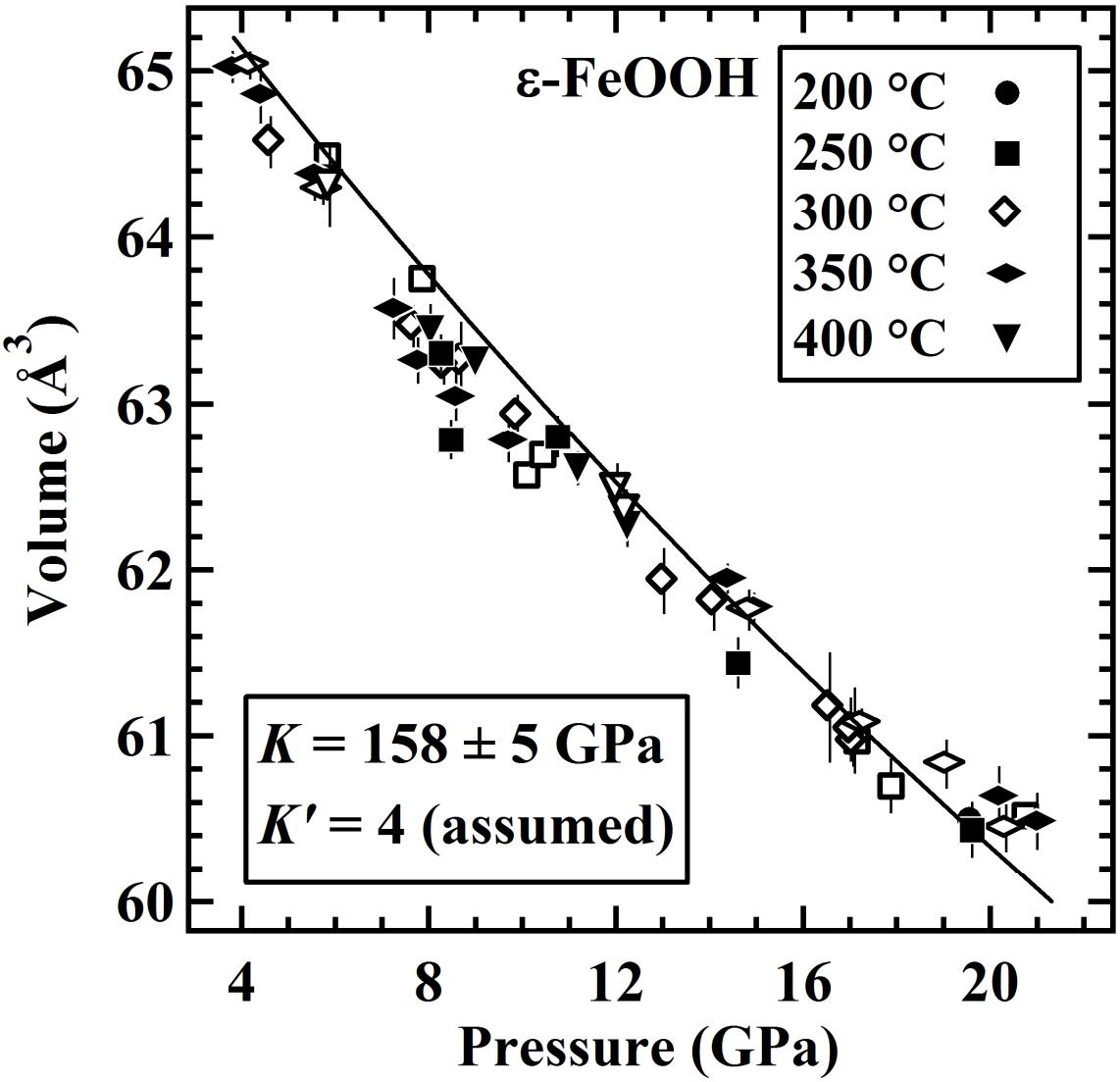
ε-FeOOH
200 °C
250 °C
300 °C
350 °C
400 °C
K = 158 ± 5 GPa
K′ = 4 (assumed)
Volume (Å3)
Pressure (GPa)
65
64
63
62
61
60
4
8
12
16
20

Figure 3b.

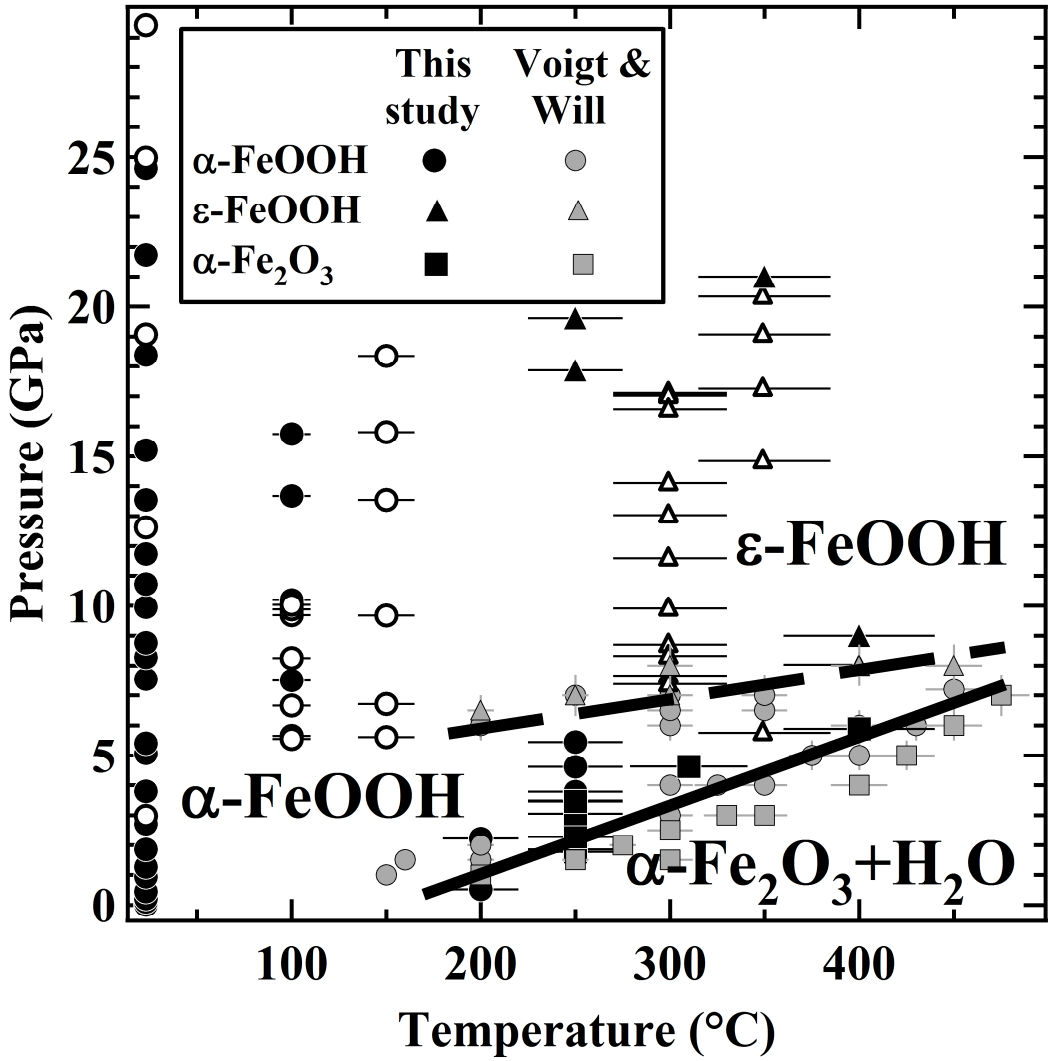
This study
Voigt & Will
α-FeOOH
ε-FeOOH
α-Fe2O3
ε-FeOOH
α-FeOOH
α-Fe2O3+H2O
Pressure (GPa)
Temperature (°C)
0
5
10
15
20
25
100
200
300
400

Figure 4.